# Chapter 14
# Surface Waves and Boundary Effects in DNLS Equations

**Ying-Ji He and Boris A. Malomed**

## 14.1 Introduction

Surface waves represent excitations which may propagate along interfaces between different media. These waves occur in diverse areas of physics, chemistry, and biology, often displaying properties that find no counterparts in bulk media [1]. The study of waves on the free surface of water and internal surfaces in stratified liquids is a classical chapter of hydrodynamics. The investigation of surface modes in solid-state physics was initiated by Tamm in 1932, who used the Kronig–Penney model to predict specific electron modes (*Tamm states*) localized at the edge of the solid [2]. This line of research was extended by Shockley in 1939 [3]. In linear optics, Kossel had predicted the existence of localized states near the boundary between homogeneous and layered media in 1966 [4], which were later observed in AlGaAs multilayer structures [5, 6]. Such waves were also shown to exist at metal–dielectric interfaces [7], as well as at interfaces between anisotropic materials [8]. In nonlinear optics, surface waves, which include transverse electric (TE), transverse magnetic (TM) and mixed polarization modes propagating at the interface between homogeneous dielectric media with different properties, were theoretically predicted in the works [9, 10] (see also review [11]).

The formation of surface solitons of the gap type (with their propagation constant falling in a bandgap of the linear spectrum generated by the respective linearized system) was predicted too [12] and observed in experiments carried out in an optical system described by such a model [13]. Surface solitons have also been predicted at an interface between two different semi-infinite waveguide arrays [14], as well as at boundaries of two-dimensional (2D) nonlinear lattices [14–18]. It has been shown that surface solitons of the vectorial [19, 20] and vortical [21] types, as well as surface kinks [22], can exist too. In addition to that, multicomponent (polychromatic) surface modes have been predicted and experimentally observed [23–25].

Y.-J. He (✉)
School of Electronics and Information, Guangdong Polytechnic Normal University, Guangzhou 510665; State Key Laboratory of Optoelectronic Materials and Technologies, Sun Yat-Sen University, Guangzhou 510275, China
e-mail: hyj8409@sxu.edu.cn

P.G. Kevrekidis, *The Discrete Nonlinear Schrödinger Equation*, STMP 232, 259–275, DOI 10.1007/978-3-540-89199-4_14, 

Closer to the main topic of the present book are *discrete* surface solitons. The existence of such localized lattice modes was first analyzed in one-dimensional (1D) arrays of nonlinear optical waveguides [26]. These states, predicted to exist at the edge of a semi-infinite array, feature a power threshold necessary for their formation, similar to that encountered by nonlinear surface waves at interfaces between continuous media [26, 27]. The formation and properties of discrete surface solitons have been explored theoretically in detail [26–32], and these solitons were quickly created in experiments performed in arrays of optical waveguides [33, 34]. Discrete surface solitons have been predicted in a number of other settings, such as those based on vectorial models [35, 36] and superlattices [37], as well as in a system with the quadratic nonlinearity [38].

In higher dimensions, 2D discrete surface solitons have been reported in theoretical and experimental forms [17, 39]. Recently, the creation of discrete solitons of a *corner type*, in a 2D array of optical waveguides confined by two orthogonal surfaces that form the corner, was reported in the work [18]. Finally, spatiotemporal discrete surface solitons have been predicted in the theoretical works [40, 41].

In this chapter, we present an outline of several basic theoretical and experimental results obtained for discrete surface solitons which can be supported by boundaries of various types. We first consider the simplest case of the surface solitons in 1D Kerr media (those with the cubic nonlinearity), starting with the underlying theory and then proceeding to the experimental realization. This will be further extended into 2D and 3D settings.

## 14.2 Discrete Nonlinear Schrödinger Equations for Surface Waves

### *14.2.1 The One-Dimensional Setting*

In a semi-infinite nonlinear lattice (in the experiment, it represents a long array of weakly coupled nonlinear optical waveguides, as schematically depicted in Fig. 14.1), the normalized field amplitudes at lattice sites $n \geq 0$ obey a discrete nonlinear Schrödinger (DNLS) equation, which incorporates the boundary condition at the surface [26],

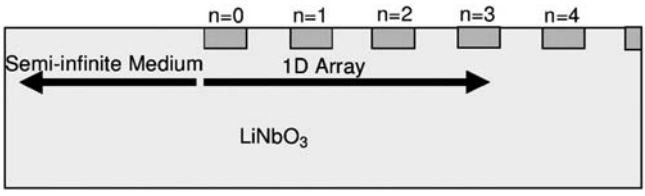


**Fig. 14.1** A typical scheme of a semi-infinite array of optical waveguides, buried into a bulk medium, which gives rise to effectively one-dimensional quasi-discrete surface solitons. Reprinted from [38] with permission

$$i\frac{d}{dz}u_0 + u_1 + \beta|u_0|^2u_0 = 0, \tag{14.1}$$

$$i\frac{d}{dz}u_n + (u_{n+1} + u_{n-1}) + \beta|u_n|^2u_n = 0. \tag{14.2}$$

In the model of the array of optical waveguides, the evolution variable $z$ is the distance of the propagation of electromagnetic signals along the waveguides, and $\beta$ is the coefficient of the on-site nonlinearity, the self-focusing and self-defocusing nonlinearities corresponding, respectively, to $\beta > 0$ and $\beta < 0$. Unless it is said otherwise, we set $\beta \equiv 1$, by means of an obvious rescaling of the lattice field. Equation (14.1) governs the evolution of the field at the edge of the array, which corresponds to site $n = 0$, and Eq. (14.2) applies at every other site, with $n \geq 1$. The actual electric field in the optical wave is expressed in terms of scaled amplitudes $u_n$ as follows: $E_n = \sqrt{2C\lambda_0\eta_0/(\pi n_0\hat{n}_2)}u_n$, where $C$ is the inter-site coupling coefficient in physical units (in Eqs. (14.1) and (14.2), normalization $C = 1$ is adopted), $\lambda_0$ is the free-space wavelength, $\eta_0$ is the free-space impedance, $\hat{n}_2$ the nonlinear Kerr coefficient, and $n_0$ the linear refractive index of the waveguides' material.

### *14.2.2 The Two-Dimensional Setting*

The model of the 2D semi-infinite array of optical waveguides with a horizontal edge, whose plane is parallel to the direction of the propagation of light in individual waveguides, is based on the accordingly modified DNLS equation for the 2D set of amplitudes $u_{m,n}(z)$ of the electromagnetic waves in the guiding cores (see, e.g., [18]):

$$i\frac{d}{dz}u_{m,n} + C(u_{m+1,n} + u_{m-1,n} + u_{m,n+1} + u_{m,n-1} - 4u_{m,n}) + |u_{m,n}|^2u_{m,n} = 0 \tag{14.3}$$

for $n \geq 0$ and all integer values of $m$. Unlike Eqs. (14.1) and (14.2), the constant accounting for inter-site coupling, $C$, is not scaled here to be 1, as it will be used in an explicit form below. Note that the corresponding coupling length in the waveguide array, which may be estimated as $z_{\text{coupling}} \sim C^{-1/2}$ in terms of Eq. (14.3), usually takes values on the order of a few millimeters, in physical units. At the surface row, which corresponds to $n = 0$ in Eq. (14.3), one should set $u_{m,-1} \equiv 0$, as there are no waveguides at $n < 0$. Equation (14.3) admits the usual Hamiltonian representation, and also conserves the total power (norm), $P = \sum_{m=-\infty}^{\infty}\sum_{n=0}^{\infty}|u_{m,n}|^2$.

### *14.2.3 The Three-Dimensional Setting*

The equations for the slow spatiotemporal evolution of the optical signal propagating in a 2D array of linearly coupled waveguides can be cast in the following form [40, 41]:

$$\left(i\frac{\partial}{\partial z}-\gamma\frac{\partial^2}{\partial\tau^2}\right)u_{m,n}+(u_{m+1,n}+u_{m-1,n}+u_{m,n+1}+u_{m,n-1}-4u_{m,n})u_{m,n}$$
$$+|u_{m,n}|^2u_{m,n}=0, \tag{14.4}$$

where $z$ is, as in Eq. (14.3), the propagation distance, while $\tau$ is the temporal variable and, accordingly, $\gamma$ is the coefficient of the temporal dispersion in each waveguiding core. In the case of the corner configuration considered in the works [40, 41], $u_{m,n} \equiv 0$ for $m \leq -1$ and $n \leq -1$.

A different type of the 3D model is possible in the case when a planar surface borders a full 3D lattice. In that case, the basic dynamical model takes the following form:

$$i\frac{d}{dz}u_{l,m,n}+(u_{l+1,m,n}+u_{l-1,m,n}+u_{l,m+1,n}+u_{l,m-1,n}+u_{l,m,n+1}+u_{l,m,n-1}$$
$$-6u_{l,m,n})u_{l,m,n}+|u_{l,m,n}|^2u_{l,m,n}=0, \tag{14.5}$$

where the 3D discrete coordinates assume the following integer values: $-\infty < l, m < +\infty$, $0 \leq n < +\infty$, and $u_{l,m,n} \equiv 0$ for $n < 0$. This equation gives rise to 3D discrete solitons of various types, and those among them which abut on the surface, or are set at a distance from it corresponding to few lattice cells, may be considered as three-dimensional surface solitons.

## 14.3 Theoretical Investigation of Discrete Surface Waves

### *14.3.1 Stable Discrete Surface Solitons in One Dimension*

Here, we outline the first theoretical prediction of 1D discrete surface solitons at the interface between an array of waveguides and a continuous medium, as in [26]. Stationary surface waves in the semi-infinite lattice system correspond to the substitution $u_n = v_n \exp(i\Lambda z)$ in Eqs. (14.1) and (14.2), where $\Lambda$ is the corresponding propagation constant, and all amplitudes $v_n$ are assumed to be positive, which corresponds to an in-phase solution. In the system under consideration, solitons can be found with values of the propagation constant falling into the *semi-infinite gap*, $\Lambda \geq 2$, where localized solutions are possible in principle.

The family of soliton solutions, found numerically by means of the relaxation method, is presented in Fig. 14.2, in the form of the dependence of the respective total power (alias norm), $P = \sum_{n=-\infty}^{+\infty} |u_n|^2$, on the propagation constant $\Lambda$. In particular, in the region of $\Lambda > 3$, the 1D surface solitons are strongly localized, and may be approximated by a simple *ansatz*, $u_n = A\exp(-np + i\Lambda t)$, where the amplitude is given by $A^2 = \Lambda/2 + \sqrt{\Lambda^2/4 - 1} \approx \Lambda - 1/\Lambda$ and $p = 2\ln A$.

The dependence plotted in Fig. 14.2 demonstrates a minimum in the $P(\Lambda)$ curve at $\Lambda = 2.998$. This feature, in turn, implies that the discrete solitons exist only above a certain power threshold, which, in the present case, is $P_{\text{thr}} = 3.27$. The situation

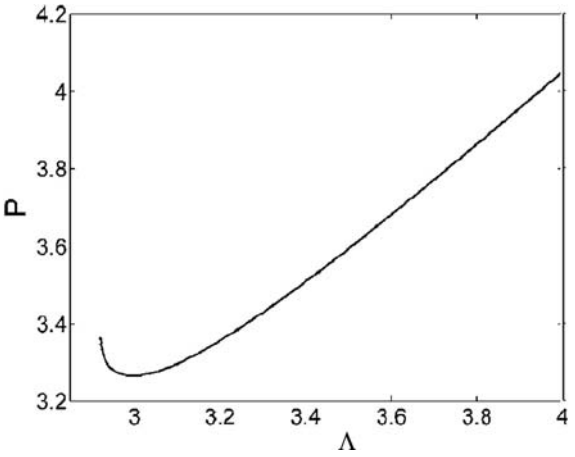


**Fig. 14.2** The total power (norm) versus propagation constant $\Lambda$ for the family of in-phase 1D discrete surface solitons. Reprinted from [26] with permission

is quite similar to that found earlier in continuum models for interfaces between nonlinear dielectric media, where the well-known Vakhitov–Kolokolov (VK) stability criterion is applicable. According to it, a necessary (but, generally speaking, not sufficient) condition for the stability of the soliton family is $dP/d\Lambda > 0$ (more accurately, the VK criterion guarantees only the absence of growing eigenmodes of infinitesimal perturbations around the solitons with a purely real growth rate, but it cannot detect unstable eigenmodes corresponding to a complex growth rate).

The full stability of these solutions was also tested in direct simulations of Eq. (14.3). Figure 14.3 demonstrates that the family of the 1D surface solitons is split into stable and unstable subfamilies – in fact, in exact accordance with the VK criterion.

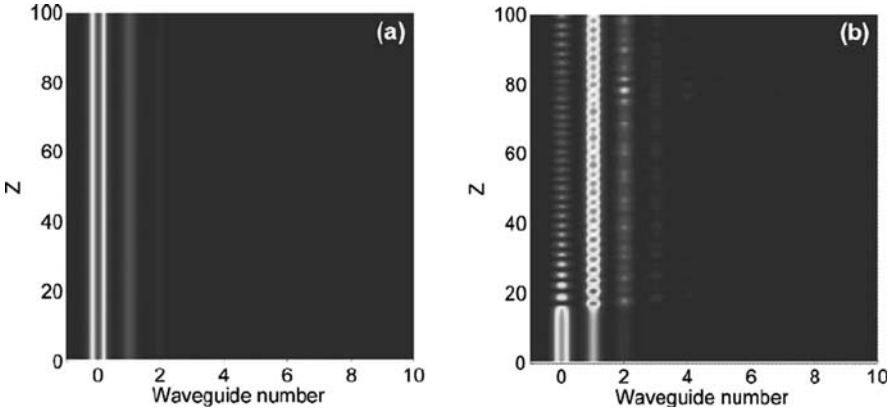


**Fig. 14.3** Examples of stable (**a**) and unstable (**b**) evolution of the 1D surface solitons for $\Lambda = 3.2$ and 2.92, respectively. Reprinted from [26] with permission

### 14.3.2 Discrete Surface Solitons at an Interface Between Self-Defocusing and Self-Focusing Lattice Media

A specific type of interface corresponds to that between two lattices, with the self-focusing and defocusing nonlinearities, i.e., $\beta > 0$ and $\beta < 0$ in Eqs. (14.1) and (14.2). Following [42], we will present here an example with $\beta_n = -0.9$ for $n < 0$ and $\beta_n = 1.1$ for $n > 0$. Discrete solitons are looked for in the same general form as above, i.e., $u_n = v_n \exp(i\Lambda t)$, where $\Lambda$ is, as before, the propagation constant, and the stationary lattice field $v_n$ obeys the following equation:

$$\Lambda v_n - C\triangle_2 v_n - \beta_n |v_n|^2 v_n = 0. \tag{14.6}$$

In the anticontinuum (AC) limit, i.e., for $C = 0$, solutions to Eq. (14.6) can be immediately constructed in the form of one or several "excited" sites carrying a nonzero amplitude, $v_n = \pm\sqrt{\Lambda/\beta_n}$ (provided that $\Lambda\beta_n > 0$), while at all other sites the amplitude is zero. Carrying out subsequent numerical continuation of the solution to $C > 0$, this approach makes it possible to generate various species of discrete solitons, seeded at $C = 0$ by the respective "skeletons."

In [42], a number of soliton families were constructed, starting, in the AC limit, from the "skeletons" of the following types: a single excited site at $n = 0$; a pair of in-phase or out-of-phase excited sites at $n = 0$ and 1; and a triplet consisting of an excited site at $n = 0$ and ones with the opposite signs at $n = 1, 2$, and similar patterns based on four- and five-site "skeletons." Figure 14.4 displays two lowest order solution branches found in this model, viz., those seeded by the single-site configuration, and the dual-site one of the in-phase type.

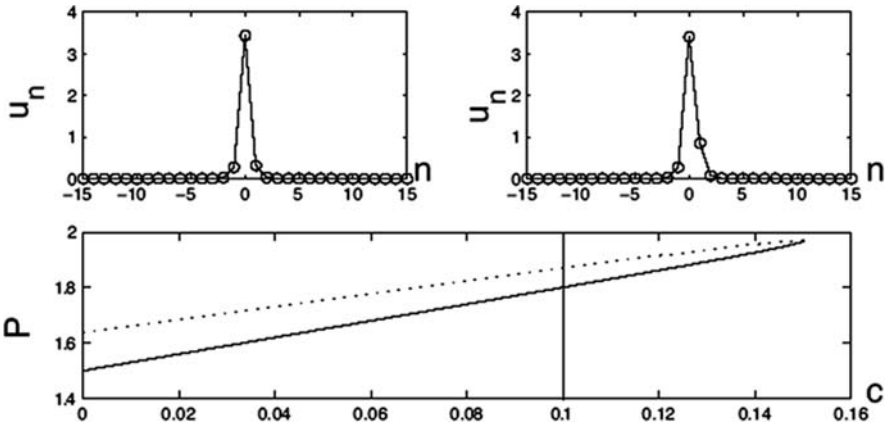


**Fig. 14.4** *Top left and right panels* display, for $C = 0.1$, examples of states near the interface between self-focusing and defocusing lattices, which are engendered, respectively, by a single excited site, or a pair of excited in-phase sites, in the anticontinuum limit ($C = 0$), as in [42]. *Bottom*: families of these solutions are presented through the dependence of their power on $C$. As usual, *the solid and dashed lines* designate stable and unstable solutions, respectively. *The vertical line* marks the examples shown in the *top panels*

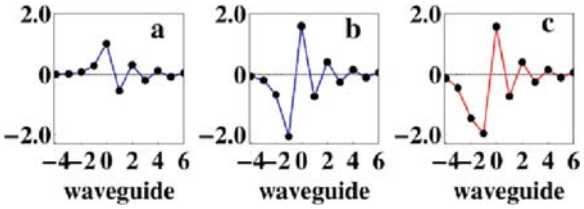


**Fig. 14.5** Examples of hybrid (unstaggered–staggered) discrete solitons, attached to the interface between lattice media with the self-focusing and defocusing nonlinearities. The solitons in panels (**a**) and (**b**) are stable, while the one in (**c**) is unstable. Reprinted from [43] with permission

As stressed in [43], the interface of the same type as considered in this subsection, i.e., between lattice media with self-focusing and self-defocusing on-site nonlinearities, may give rise to *hybrid solitons*. They look as unstaggered and staggered states on the two sides of the interface, see examples in Fig. 14.5. Probably, similar hybrid states can be found in 2D and 3D models including an interface between self-focusing and self-defocusing nonlinearities.

### *14.3.3 Tamm Oscillations of Unstaggered and Staggered Solitons*

Here we outline the theoretical prediction of *Tamm oscillations* of discrete solitons created near the edge of a 1D lattice (of optical waveguides), following [31]. These are oscillations of the position of a narrow soliton, due to the interplay of its repulsion from the lattice's edge and Bragg reflection from the bulk of the lattice (see below).

The analysis starts with the discrete equation for the propagation of light in the array, cf. Eqs. (14.1) and (14.2):

$$i\frac{d}{dz}u_n + C(u_{n+1} + u_{n-1} - 2u_n) + g|u_n|^2 u_n = 0, \tag{14.7}$$

where $C$ is, as above, the lattice-coupling constant, while $g(|u_n|^2) = \beta|u_n|^2$ and $g(|u_n|^2) = \beta|u_n|^2/(1 + |u_n|^2)$ in cubic and saturable media, respectively, with nonlinearity coefficient $\beta > 0$ and $\beta < 0$ corresponding to the self-focusing and self-defocusing signs of the nonlinearity. The boundary conditions added to Eq. (14.7) are the same ones as considered above, see Eq. (14.1).

Stationary solutions to Eq. (14.7) are looked for in the usual (*unstaggered*) form, $u_n = v_n \exp(-i\Lambda t)$, in the case of the self-focusing, and in the *staggered* form, with alternating signs of the stationary fields at adjacent sites of the lattice, in the opposite case. The staggering substitution, $u_n = v_n(-1)^n \exp(i\Lambda z)$, makes the self-defocusing nonlinearity equivalent to its self-focusing counterpart. Staggered solitons, which may be found in various models with self-defocusing, may also be regarded as *gap solitons*, as they exist at values of the propagation constant which fall in one of finite bandgaps in the spectrum of the corresponding linearized model.

On the contrary to that, the propagation constant of ordinary – unstaggered – solitons belongs to the semi-infinite spectral gap.

Assuming that solitons generated by Eq. (14.7) are narrow (strongly localized), one can construct analytical approximations for two different types of such solitons, on-site-centered and inter-site-centered ones. The solutions of the former type have the largest value of the field at the edge, $n = 0$, with the lattice field decaying as $v_n \approx \alpha^n v_0$ at $n > 0$. Inter-site-centered solitons feature the largest local amplitude at $n = 1$, and decay as $v_n \approx \alpha^{n-1} v_1$ for $n > 1$. In either case, the localization of the soliton is determined by a small parameter, $\alpha = C/(\Lambda + 2C)$.

In direct simulations of Eq. (14.7), these narrow solitons feature swinging motions, as shown in Fig. 14.6, which are the Tamm oscillations of the narrow solitons, staggered and unstaggered ones. The oscillations are not quite persistent: in the course of its motion in the lattice, the soliton gradually loses energy due to emission of linear waves ("lattice radiation," alias "phonons"), which leads to gradual damping of the oscillations. Eventually, the soliton comes to a halt at a position at some distance from the surface (the distance may be as small as two lattice sites, see further details in [31]).

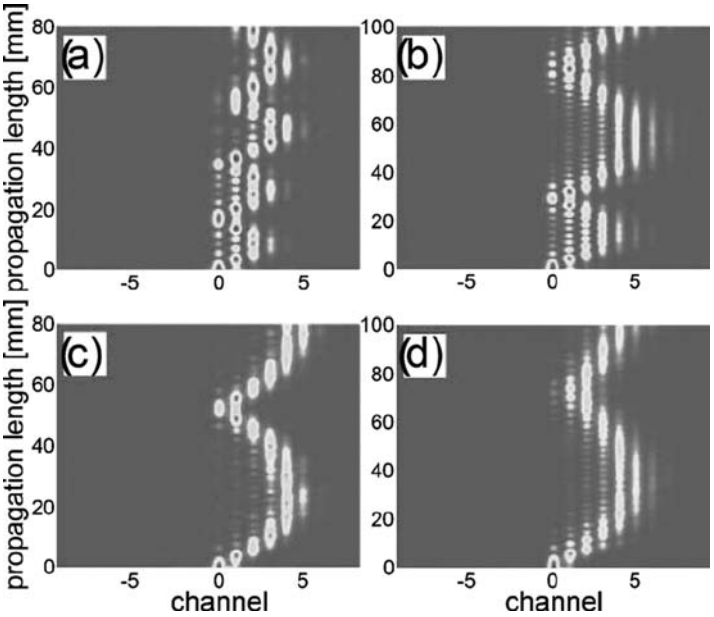


**Fig. 14.6** Examples of Tamm oscillations of several types of narrow discrete solitons created near the edge of the lattice. The simulations were performed for typical values of parameters corresponding to arrays of nonlinear optical waveguides in the following models: (**a**) self-defocusing saturable, (**b**) self-defocusing cubic, (**c**) self-focusing saturable, and (**d**) self-focusing cubic. In panels (a) and (b), the soliton is staggered (otherwise, it cannot exist in the defocusing medium), while in (c) and (d) it is the usual unstaggered soliton. Reprinted from [31] with permission

For the interpretation of the oscillations, it is relevant to notice that the edge of the lattice (the surface) induces an effective repulsive potential acting on the narrow discrete soliton. Stronger inter-site coupling results in the stronger surface-induced potential, while enhanced nonlinearity suppresses it [31]. Then, Tamm oscillations of the soliton may be understood as oscillations in the effective Peierls–Nabarro (PN) potential, induced by the underlying lattice, under the action of the additional repulsive potential. In other words, the oscillations are a result of the interplay of the repulsion of the soliton from the lattice surface and Bragg reflection in the depth of the lattice. The combination of the edge-induced and PN potentials gives rise to a stable equilibrium position of the soliton at a finite distance from the edge, where the soliton eventually gets trapped.

### *14.3.4 Discrete Surface Solitons in Two Dimensions*

The aim of this subsection is to present an outline of the theoretical prediction of 2D discrete surface solitons at the interface between a 2D lattice of optical waveguides and a substrate, following [39]. The model is based on Eq. (14.3), stationary solutions to which are looked for as $u_{m,n} = \exp(i\Lambda z)v_{m,n}$, with $\Lambda$ scaled to be 1, and the stationary lattice distribution obeying the respective equation, $(1 - |v_{m,n}|^2)v_{m,n} - C(v_{m,n+1} + v_{m,n-1} + v_{m+1,n} + v_{m-1,n} - 4v_{m,n}) = 0$.

In [39], it was shown that the interaction with the edge expands the stability region for fundamental solitons, and induces a difference between dipoles (bound states of two fundamental lattice solitons with opposite signs) oriented perpendicular and parallel to the surface. A notable finding is that the edge supports a species of localized patterns which exists too but is *always unstable* in the uniform lattice, namely, a horseshoe-shaped soliton. As shown in Fig. 14.7, the "skeleton" of the horseshoe structure consists of three lattice sites.

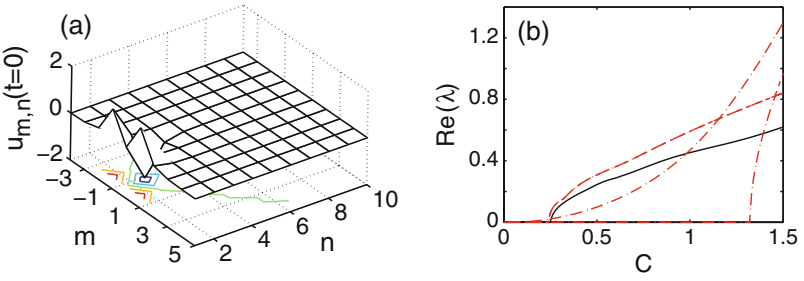


**Fig. 14.7** (**a**) An example of the 2D surface soliton of the "horseshoe" type, as in [39]. *The solid curve* in panel (**b**) displays the real part of a critical instability eigenvalue for the soliton family of this type. For comparison, *the dashed–dotted lines* in (b) show the instability eigenvalues for the horseshoe family in the uniform lattice (without the edge). The latter family is completely (although weakly) unstable, due to a very small nonzero eigenvalue extending to $C = 0$, while the horseshoes trapped at the edge of the lattice have a well-defined stability region – in the present case, it is, approximately, $C < 0.25$

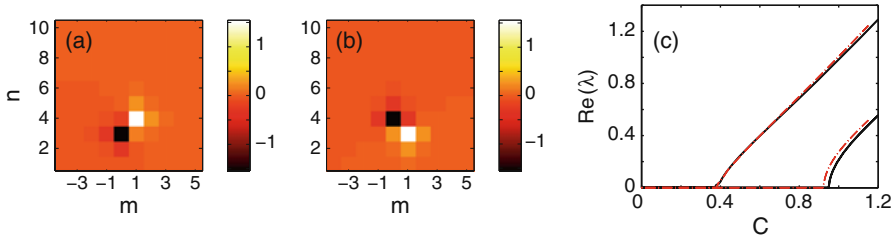


**Fig. 14.8** An example of a supersymmetric vortex cell. Panels **(a)** and (**b)** show, respectively, the real and imaginary parts of the solution. In panel **(c)**, *the solid lines* show instability eigenvalues of these states, as in [39]. For comparison, *dashed–dotted lines* depict the same numerically found characteristics for the supersymmetric vortex in the infinite lattice (the one without the edge)

The edge of the 2D lattice may also act in an opposite way, *impeding* the existence of localized solutions of other types. A relevant example of that is provided the so-called supersymmetric lattice vortex, i.e., one with the intrinsic vorticity ($S = 1$) equal to the size of the square (a set of four excited sites) which seeds the vortex at $C = 0$ in the above-mentioned *AC limit* (i.e., for the lattice composed of uncoupled sites), as shown in Fig. 14.8a, b. The configuration displayed in the figure is placed at the minimum separation from the edge admitting its existence, which amounts to two lattice sites. Numerically found stability eigenvalues for this structure are presented in Fig. 14.8c.

The numerical analysis of 3D equation (14.5) reveals similar effects for several species of discrete 3D solitons. In particular, three-site horseshoes are also completely unstable in the bulk 3D lattice, but are stabilized if they abut upon the lattice's surface. As for 3D vortex solitons, their properties strongly depend on the orientation with respect to the surface: the ones set parallel to the surface are essentially stabilized by it, while localized vortices with the perpendicular orientation cannot exist close to the surface.

### *14.3.5 Spatiotemporal Discrete Surface Solitons*

The theoretical prediction of spatiotemporal discrete surface solitons at the interface between a lattice of optical waveguides and a continuous medium was reported in [40, 41], using the model based on Eq. (14.4). Stationary solutions for a spatiotemporal soliton can be looked as $u_{m,n}(z,\tau) = v_{m,n}(\tau)\exp(i\Lambda z)$, where envelopes $v_{m,n}(\tau)$ describe the temporal shape of soliton-like pulses at lattice sites $(n, m)$. Several examples of the spatiotemporal solitons found in [40, 41] by means of numerical methods in the lattice with the corner are shown in Fig. 14.9.

### *14.3.6 Finite Lattices and the Method of Images*

In both 1D and 2D settings, some of the results outlined above can also be obtained by means of the *method of images*. For instance, in the 1D case with the *fixed* (zero)

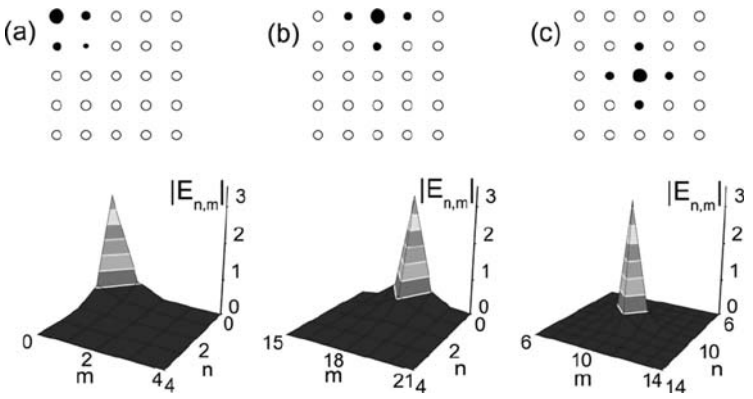


**Fig. 14.9** *Top*: Panels (**a**)–(**c**) display typical examples of spatiotemporal modes localized at the lattice's corner, at the edge, and in the center of the lattice. *Bottom*: Spatial cross sections of the corresponding stable spatiotemporal solitons. Reprinted from [40, 41] with permission

boundary condition, i.e., $u_n = 0$ for $n \leq -1$ (see Eqs. (14.1) and (14.2)), the solution is equivalent to that in an infinite lattice which is subject to the anti-symmetry constraint, $u_{-(n+2)} \equiv -u_n$, $n = -1, 0, +1, +2, ...$ (which, obviously, includes condition $u_{-1} \equiv 0$ ). This way of the extension of the semi-infinite lattice into the full infinite one implies that a localized excitation created at a lattice site with number $m$ comes together with its image, of the opposite sign, placed at site $-(m + 2)$, as shown in Fig. 14.10. In [44], the image method was also elaborated in detail (but chiefly within the framework of linear models) for 2D lattices, including corner- and sector-shaped ones.

The same method may be applied to finite lattices, which are composed of a finite number of sites between two edges. An example of such a configuration was investigated in detail for discrete solitons in [45] – not in terms of the DNLS equation, but rather for solitons in the Ablowitz–Ladik (AL) model, which is based on the following discrete equation, $idu_n/dz = -(u_{n+1} + u_{n-1})(1 + |u_n|^2)$. The infinite AL lattice, as well as a finite one subject to periodic boundary conditions, are integrable systems. Under the fixed boundary conditions ($u_n \equiv 0$ for $n \geq N + 1$ and $n \leq -(N + 1)$, if the truncated lattice consists of $2N + 1$ sites), the integrability is lost. For this case, an effective potential accounting for the interaction of a soliton (which is treated as a quasi-particle) with the edges was derived in

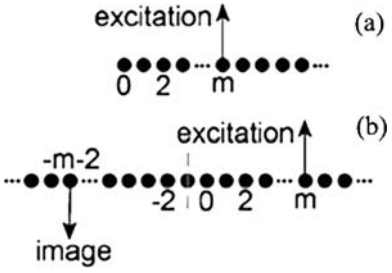


**Fig. 14.10** (**a**) A semi-infinite lattice with local excitation at site $m$; (**b**) the equivalent configuration,with the negative image at site $-(m + 1)$, in the respective infinite lattice. Reprinted from [44] with permission

[45], and it was demonstrated that this effective potential predicts oscillations of the soliton in the finite AL lattice with a very good accuracy, if compared to direct simulations.

Finally, it is worth mentioning that the stability and instability of solitons in 1D and 2D DNLS lattices with an edge can be understood, in terms of the interaction of the soliton with its image, as manifestations of the general results for the stability and instability of bound states of two solitons with opposite or identical signs, that were reported in the works [46, 47].

## 14.4 Experimental Results

### *14.4.1 Discrete Surface Solitons in One Dimension*

The first experimental observations of discrete surface solitons at the edge of a lattice of nonlinear optical waveguides were reported in [33, 34] (the material used to build the corresponding setup was AlGaAs, which is known for a very large value of the Kerr coefficient). The corresponding experimental configuration is shown in Fig. 14.11a. Its parameters were close to those previously used to observe discrete highly localized Kerr solitons in the bulk lattice (far from the edges). The array contained 101 cores and was 1 cm long, while the coupling length, determined by the linear interaction between adjacent cores, was estimated to be 2.2 mm. A set of experiments and simulations dealing with the excitation of the channel (core) at the edge of the array ($n = 0$) is depicted in Fig. 14.11.

### *14.4.2 Staggered Modes*

The experimental observation of *staggered* discrete modes at the interface between a waveguide array, built of a copper-doped LiNb crystal, and a continuous medium was reported in [32]. The experimental sample contained 250 parallel waveguides. The width and height of the single-mode channel waveguides were 4 and 2.5 μm, respectively, while the distance between adjacent channels was 4.4 μm, the corresponding coupling length being 1.1 mm.

Optical beams of equal power, overlapping under a small angle, were coupled into the waveguide array, taking care to make the grating period of the resulting interference pattern matching the period of the array (which is 8.4 μm, according to what was said above). This input pattern had an elliptical shape whose height was adjusted to match the depth of each waveguide (approximately 2.5 μm).

In this way, a staggered input pattern was created. It consisted of a central maximum and a small number of satellites with alternating signs. The sample was placed so as to match the maximum of the staggered input and the first channel of the array. The experimental results are plotted in Fig. 14.12.

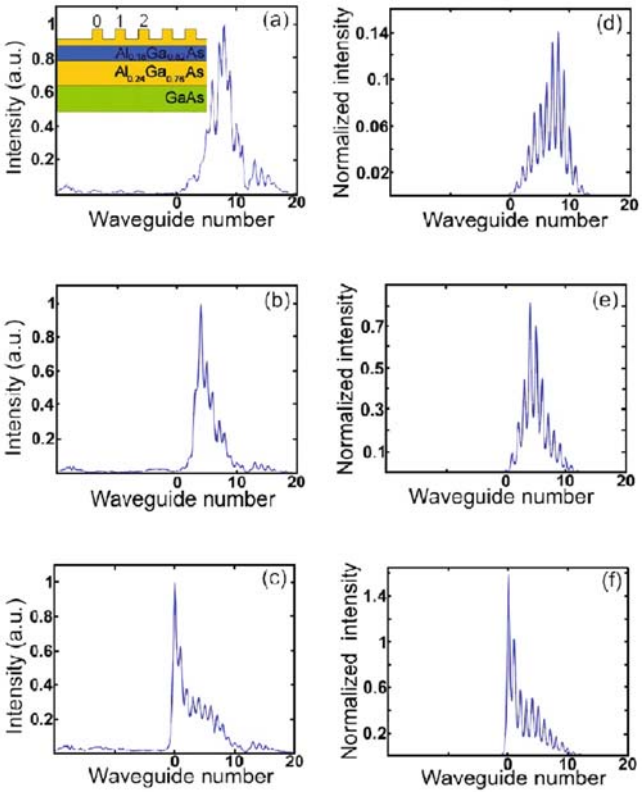


**Fig. 14.11** Intensity patterns observed in the experiments and numerical simulations reported in [33, 34] (reprinted with permission) at the output of the AlGaAs waveguide array, for three different values of the power of the beam injected into channel $n = 0$. *Left-hand side*: experimental results for (**a**) $P = 450$ W, (**b**) $P = 1300$ W, and (**c**) $P = 2100$ W. *Right-hand side*: results of the numerical simulations for (**d**) $P = 280$ W, (**e**) $P = 1260$ W, and (**f**) $P = 2200$ W. The inset in panel (a) displays the experimental setup

### *14.4.3 Discrete Surface Solitons in Two Dimensions*

Experimental observations of 2D optical discrete surface solitons were reported in [17] and [18]. Here, we summarize the results of the work [17], which used the interface between a *virtual* (photoinduced) waveguide array, created in an SBN photorefractive crystal, and a uniform medium.

The application of the positive bias voltage to a 10-mm-long sample of the crystal induced sufficiently strong self-focusing nonlinearity in the medium, and thus made it possible to create in-phase lattice surface solitons. Typical experimental results are shown in Fig. 14.13, where panel (a) displays a part of the underlying lattice pattern. The discrete diffraction in this case is stronger in the direction perpendicular to the edge than in the direction parallel to it, as seen in Fig. 14.13b. For a sufficiently high bias voltage, the self-action of the input beam provided for the formation of a

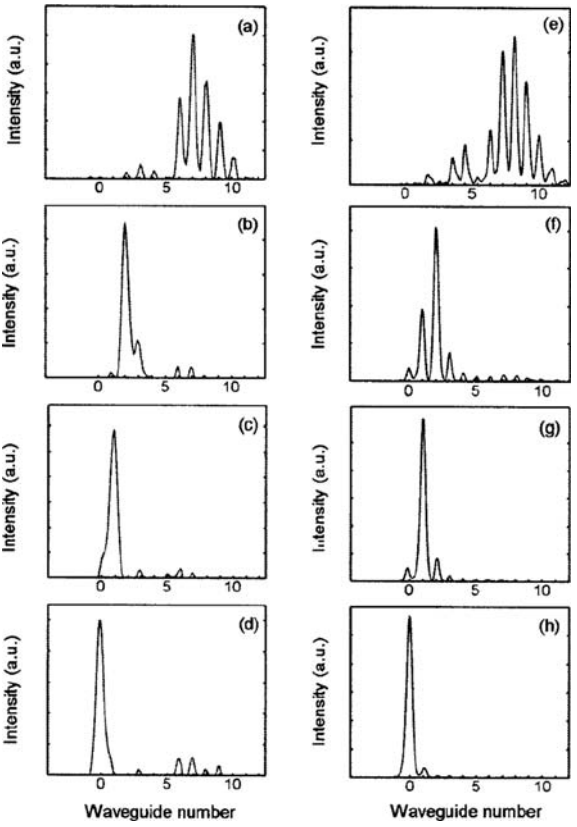


**Fig. 14.12** Output patterns corresponding to the staggered input excitation of three channels, with intensity ratio 1:0.5:0.1, as reported in [32] (reprinted with permission). The results are shown for four different input powers. *Left column*: experimental results for (**a**) discrete diffraction (low-power linear regime), (**b**) power $P = 9\ \mu$W, (**c**) $P = 22.5\ \mu$W, and (**d**) $P = 225\ \mu$W. *Right column*: results of respective numerical simulations for (**e**) the linear discrete diffraction, (**f**) $P = 10\ \mu$W, (**g**) $P = 22\ \mu$W, and (**h**) $P = 230\ \mu$W

discrete surface soliton, see Fig. 14.13c, d. On the other hand, if the intensity of the beam was reduced by a factor of $\geq 8$, it was not able to form a soliton, undergoing strong discrete diffraction at the surface, as seen in Fig. 14.13h. In the same work [17], 2D surface solitons were also observed at the corner of the 2D lattice, as shown in Fig. 14.13e–g.

The application of the negative bias voltage turned the crystal into a self-defocusing medium, which made it possible to create staggered 2D surface solitons, which belong to the first bandgap of the respective lattice-induced linear spectrum. With the appropriate defocusing nonlinearity, a surface *gap soliton* could be created, using a single input beam.

The difference between the in-phase surface solitons (see Fig. 14.13i, j) and staggered ones (Fig. 14.13k, l) may be clearly illustrated by the interference fringes, which break and interleave in the latter case, as shown in Fig. 14.13l. The power spectrum for the staggered solitons was also drastically different from that of the in-phase surface solitons.

Typical results of numerical simulations of the model corresponding to the experiment are presented in the right panels of Fig. 14.13, where the top one shows 3D

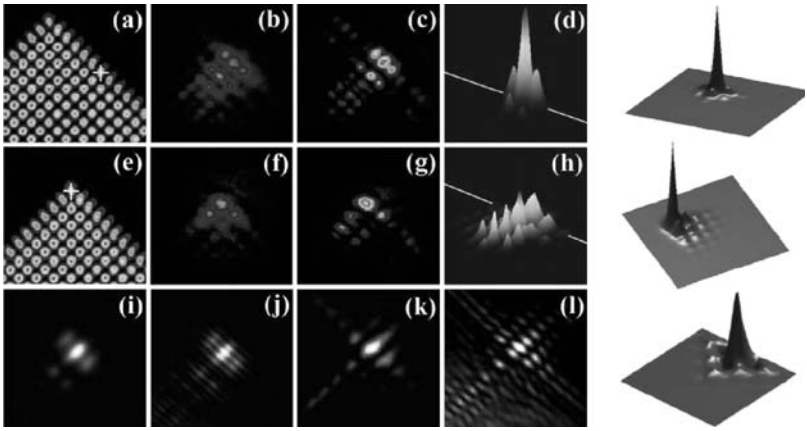


**Fig. 14.13** The formation of discrete 2D surface solitons at the lattice edge (**a–d**) and lattice corner (**e–g**). Adapted from [17] with permission

plots of the 2D surface soliton at the lattice edge, corresponding to Fig. 14.13d, the middle panel shows the predicted surface soliton at the lattice corner corresponding to Fig. 14.13g, and the bottom panel presents the prediction for the surface gap soliton corresponding to Fig. 14.13k. Small dips around the central peak in the bottom figure indicate the staggered phase structure of the corresponding surface soliton.

## 14.5 Conclusions

In this chapter, basic theoretical and experimental results for discrete surface (and corner) solitons in lattices with the cubic on-site nonlinearity were summarized, in terms of 1D and 2D semi-infinite arrays of optical waveguides. Theoretical predictions for spatiotemporal corner solitons were presented too, as well as for 2D surface solitons with a nontrivial intrinsic structure, such as localized discrete vortices and "horseshoes." Solitons of both the in-phase (unstaggered) and staggered types have been considered (solitons of the staggered type, which are supported by the self-defocusing nonlinearity, are also called gap solitons).

As predicted theoretically and demonstrated experimentally, these solitons demonstrate various noteworthy phenomena such as power thresholds, Tamm oscillations (which are akin to Bloch oscillations), and the stabilization by the lattice edge of localized structures (such as 2D and 3D "horseshoes") which cannot be stable in bulk lattices.

Theoretical and experimental studies of surface and corner solitons can be extended in various directions. In particular, the analysis of surface states in full 3D models has started very recently. Dynamical 3D bulk lattices of the DNLS type (with the cubic on-site nonlinearity) give rise to many species of stable discrete solitons with specific arrangements and topological features, that have no counterparts in

lower dimensions. These include octupoles, diagonal vortices, vortex "cubes" (stack of two quasiplanar vortices) "diamonds" (formed by two mutually orthogonal vortices) [48, 49], and discrete quasi-Skyrmions of a toroidal shape (that were found together with 2D discrete patterns of the "baby-Skyrmion" type) [50]. An obvious possibility is to investigate such 3D objects when they are placed on or close to the edge of the 3D lattice.

Virtually unexplored surfaces remain of 2D and 3D lattices whose shape is different from the simplest square and cubic types (such as triangular and hexagonal lattices in two dimensions). On the other hand, it may also be interesting to study surface states in 2D and 3D models with the quadratic (rather than cubic) on-site nonlinearity. Another challenging issue is a possibility to find 2D and, possibly, 3D discrete solitons attached to the lattice's surface that would feature *mobility* along the surface.

## References


1. Zangwill, A.: Physics at Surfaces, Cambridge University Press, Cambridge (1988) 259
2. Tamm, I.: Phys. Z. Sowjetunion **1**, 733 (1932) 259
3. Shockley, W.: Phys. Rev. **56**, 317 (1939) 259
4. Kossel, D.: J. Opt. Soc. Am. **56**, 1434 (1966) 259
5. Yeh, P., Yariv, A., Cho, A.Y.: Appl. Phys. Lett. **32**, 104 (1978) 259
6. Ng, W., Yeh, P., Chen, P.C., Yariv, A.: Appl. Phys. Lett. **32**, 370(1978) 259
7. Barnes, W.L., Dereux, A., Ebbesen, T.W.: Nature **424**, 824 (2003) 259
8. Artigas, D., Torner, L.: Phys. Rev. Lett. **94**, 013901 (2005) 259
9. Seaton, C.T., Valera, J.D., Shoemaker, R.L., Stegeman, G.I., Chilwell, J.T., Smith, S.D.: IEEE J. Quantum Electron. **21**, 774 (1985) 259
10. Mihalache, D., Stegeman, G.I., Seaton, C.T., Wright, E.M., Zanoni, R., Boardman, A.D., Twardowski, T.: Opt. Lett. **12**, 187 (1987) 259
11. Mihalache, D., Bertolotti, M., Sibilia, C.: Prog. Opt. **27**, 229 (1989) 259
12. Kartashov, Y.V., Vysloukh, V.A., Torner, L.: Phys. Rev. Lett. **96**, 073901 (2006) 259
13. Rosberg, C.R., Neshev, D. N., Krolikowski, W., Mitchell, A., Vicencio, R.A., Molina, M.I., Kivshar, Y.S.: Phys. Rev. Lett. **97**, 083901 (2006) 259
14. Makris, K.G., Hudock, J., Christodoulides, D.N., Stegeman, G.I., Manela, O., Segev, M.: Opt. Lett. **31**, 2774 (2006) 259
15. Kartashov, Y.V., Vysloukh, V.A., Mihalache, D., Torner, L.: Opt. Lett. **31**, 2329 (2006) 259
16. Kartashov, Y.V., Torner, L.: Opt. Lett. **31**, 2172 (2006) 259
17. Wang, X., Bezryadina, A., Chen, Z., Makris, K.G., Christodoulides, D.N., Stegeman, G.I.: Phys. Rev. Lett. **98**, 123903 (2007) 259, 260, 271, 272, 273
18. Szameit, A., Kartashov, Y.V., Dreisow, F., Pertsch, T., Nolte, S., Tunnermann, A., Torner, L.: Phys. Rev. Lett. **98**, 173903 (2007) 259, 260, 261, 271
19. Kartashov, Y.V., Ye, F., Torner, L.: Opt. Express **14**, 4808 (2006) 259
20. Garanovich, I.L., Sukhorukov, A.A., Kivshar, Y.S., Molina, M.: Opt. Express **14**, 4780 (2006) 259
21. Kartashov, Y.V., Vysloukh, V.A., Egorov, A.A., Torner, L.: Opt. Express **14**, 4049 (2006) 259
22. Kartashov, Y.V., Vysloukh, V.A., Torner, L.: Opt. Express **14**, 12365 (2006). 259
23. Motzek, K., Sukhorukov, A.A., Kivshar, Y.S.: Opt. Express **14**, 9873 (2006) 259
24. Motzek, K., Sukhorukov, A.A., Kivshar, Y.S.: Opt. Lett. **31**, 3125 (2006) 259
25. Sukhorukov, A.A., Neshev, D.N., Dreischuh, A., Fischer, R., Ha, S., Krolikowski, W., Bolger, J., Mitchell, A., Eggleton, B.J., Kivshar, Y.S.: Opt. Express **14**, 11265 (2006) 259

26. Makris, K.G., Suntsov, S., Christodoulides, D.N., Stegeman, G.I., Hache, A.: Opt. Lett. **30**, 2466 (2005) 260, 262, 263
27. Suntsov, S., Makris, K.G., Christodoulides, D.N., Stegeman, G.I., Morandotti, R., Yang, H., Salamo, G., Sorel, M.: Opt. Lett. **32**, 3098 (2007) 260
28. Molina, M.I., Garanovich, I.L., Sukhorukov, A.A., Kivshar, Y.S.: Opt. Lett. **31**, 2332 (2006) 260
29. Molina, M.I., Vicencio, R.A., Kivshar, Y.S.: Opt. Lett. **31**, 1693 (2006) 260
30. Mihalache, D., Mazilu, D., Lederer, F., Kivshar, Y.S.: Opt. Express **15**, 589 (2007) 260
31. Stepić, M., Smirnov, E., Rüter, C.E., Kip, D., Maluckov, A., Hadžievski, L.: Opt. Lett. **32**, 823 (2007) 260, 265, 266, 267
32. Smirnov, E., Stepić, M., Rüter, C.E., Kip, D., Shandarov, V.: Opt. Lett. **31**, 2338 (2006) 260, 270, 272
33. Suntsov, S., Makris, K.G., Christodoulides, D.N., Stegeman, G.I., Hache, A., Morandotti, R., Yang, H., Salamo, G., Sorel, M.: Phys. Rev. Lett. **96**, 063901 (2006) 260, 270, 271
34. Suntsov, S., Makris, K.G., Siviloglou, G.A., Iwanow, R., Schiek, R., Christodoulides, D.N., Stegeman, G.I., Morandotti, R., Yang, H., Salamo, G., Volatier, M., Aimez, V., Ares, R., Sorel, M., Min, Y., Sohler, W., Wang, X.S., Bezryadina, A., Chen, Z.: J. Nonlin. Opt. Phys. Mat. **16**, 401 (2007) 260, 270, 271
35. Hudock, J., Suntsov, S., Christodoulides, D.N., Stegeman, G.I.: Opt. Express **13**, 7720 (2005) 260
36. Garanovich, L., Sukhorukov, A.A., Kivshar, Y.S., Molina, M.: Opt. Express **14**, 4780 (2006) 260
37. He, Y.J., Chen, W.H., Wang, H.Z., Malomed, B.A.: Opt. Lett. **32**, 1390 (2007) 260
38. Siviloglou, G.A., Makris, K.G., Iwanow, R., Schiek, R. Christodoulides, D.N., Stegeman, G.I.: Opt. Express **14**, 5508 (2006) 260
39. Susanto, H., Kevrekidis, P.G., Malomed, B.A., Carretero-González, R., Frantzeskakis, D.J.: Phys. Rev. E **75**, 056605 (2007) 260, 267, 268
40. Mihalache, D., Mazilu, D., Lederer, F., Kivshar, Y.S.: Opt. Lett. **32**, 3173 (2007) 260, 261, 262, 268, 269
41. Mihalache, D., Mazilu, D., Kivshar, Y., Lederer, F.: Opt. Express **15**, 10718 (2007) 260, 261, 262, 268, 269
42. Machacek, D.L., Foreman, E.A., Hoq, Q.E., Kevrekidis, P.G., Saxena, A., Frantzeskakis, D.J., Bishop, A.R.: Phys. Rev. E **74**, 036602 (2006) 264
43. Molina, M.I., Kivshar, Y.S.: Phys. Lett. A **362**, 280 (2007) 265
44. Makris, K.G., Christodoulides, D.N.: Phys. Rev. E **73**, 036616 (2006) 269
45. Rasmussen, K.Ø., Cai, D., Bishop, A.R., Grønbech-Jensen, N.: Phys. Rev. E **55**, 6151 (1997) 269, 270
46. Kapitula, T., Kevrekidis, P.G., Malomed, B.A.: Phys. Rev. E **63**, 036604 (2001) 270
47. Kevrekidis, P.G., Malomed, B.A., Bishop, A.R.: J. Phys. A Math. Gen. **34**, 9615 (2001) 270
48. Kevrekidis, P.G., Malomed, B.A., Frantzeskakis, D.J., Carretero-González, R.: Phys. Rev. Lett. **93**, 080403 (2004) 274
49. Carretero-González, R., Kevrekidis, P.G., Malomed, B.A., Frantzeskakis, D.J.: Phys. Rev. Lett. **94**, 203901 (2005) 274
50. Kevrekidis, P.G., Carretero-González, R., Frantzeskakis, D.J., Malomed, B.A., Diakonos, F.K.: Phys. Rev. E **75**, 026603 (2007) 274